International Journal of Technology

http://ijtech.eng.ui.ac.id

Research Article

A Unified Long-Haul Optical Fiber Architecture for Simultaneous High-Speed Communication and Fiber Bragg Grating-Based Sensing

Mustika Fitriana Dewi[1], Muhammad Yusha Firdaus[1], Maratul Hamidah[1], Rahmayati Alindra[1], Amalia Irma Nurwidya[1], Tinova Pramudya[1], Muhamad Asvial[2], Agus Muhamad Hatta[3], Sasono Rahardjo[1,*]

[1]Research Organization for Energy and Manufacturing, National Research and Innovation Agency, Kawasan PUSPIPTEK, Building 720, Serpong, South Tangerang, 15314, Banten, Indonesia

[2]Department of Electrical Engineering, Universitas Indonesia, Kampus Baru UI, Depok 16424, Indonesia

[3]Department of Engineering Physics, Faculty of Industrial Technology and Systems Engineering, Institut Teknologi Sepuluh Nopember (ITS), Surabaya 60111, Indonesia

[*]Corresponding author: sasono.rahardjo@brin.go.id; Tel.: +62811-1933-3639

Abstract: The integration of long-haul high-speed optical communication and distributed sensing within a single optical fiber represents a crucial step toward more efficient and scalable infrastructure for real-time environmental observation and data delivery. This study examines the performance of a 120 km single-mode optical link operating at 10 Gbps, embedded with three fiber Bragg grating (FBG) sensors positioned at 30 km intervals, enabling dual functionality over a shared single strand of physical medium. A broadband amplified spontaneous emission (ASE) source is employed to simultaneously provide the 1550 nm data channel and interrogation wavelengths at 1554, 1556, and 1558 nm for the FBG sensors. System performance is assessed using standard optical communication metrics, i.e., Q-factor, bit error rate (BER), and eye diagram analysis, while sensor reliability is evaluated through reflected signal levels and wavelength shifts captured at the receiver. The results demonstrate that sensor integration introduces no significant degradation in the transmission quality. The proposed system maintained robust performance, achieving a Q-factor of 6.38 and a BER of 6.23×10^{-11} under post compensation configuration of the dispersion compensating fiber (DCF). All FBG reflection signals remain clearly distinguishable and maintain effective responsiveness to temperature variations, confirming the feasibility of concurrent distributed sensing. By unifying sensing and high-speed communication in a long-haul link, this work thereby minimizing component count, cost, and complexity, establishing a practical foundation for next-generation scientific monitoring and reliable telecommunications (SMART) infrastructure.

Keywords: Fiber bragg grating; Dual-function optical fiber system; Distributed sensing; Long-haul communication; Scientific monitoring and reliable telecommunication infrastructure

1. Introduction

The ocean remains central to the planet's ecological balance, yet our capacity to monitor it comprehensively, particularly across the sea floor, continues to face limitations. Emerging technologies are addressing this gap through scientific monitoring and reliable telecommunications (SMART) systems, which combine environmental sensing and high-speed communication in an optical fiber telecommunication system infrastructure. By embedding sensors directly into submarine telecommunication cables, these systems offer a practical and scalable approach for continuous ocean observation on a global scale (Sifón, 2024; Howe et al., 2022; Howe et al., 2019). Various studies have investigated the use of environmental sensors to produce high-quality data crucial for climate research, sea-level tracking, and early warning systems for seismic and tsunami

https://doi.org/10.14716/ijtech.v16i6.7931
Received July 2025; Revised July 2025; Accepted September 2025

events, each requiring precise and extensive datasets (Nor et al., 2023; Marra et al., 2022; Min et al., 2021; Suastika et al., 2019).

Within the SMART framework, optical fiber sensors emerge as advantageous instruments for applications in environmental monitoring and long-haul telecommunications. These sensors offer notable benefits, such as non-invasive detection, exceptional sensitivity, resilience under harsh environmental conditions, enhanced data security, capability for simultaneous multiparameter detection, and efficacy in long-distance measurements without significant signal degradation (Elsherif et al., 2022; Pendão and Silva, 2022; Priambodo et al., 2015), making them ideal for integration with high-speed long-haul optical communication infrastructures. As one of optical fiber sensors, Fiber Bragg Grating (FBG) provides real-time, multiparameter monitoring which is sensitive to strain, temperature, pressure, and vibration (Madani et al., 2023; Wang et al., 2023; Yu et al., 2023; de la Torre et al., 2021; Sahota et al., 2020). Despite these advantages, the successful integration of sensing and communication requires careful system-level design, particularly over long-haul links. Optical impairments, such as chromatic dispersion, remain critical challenges that can compromise data integrity and sensor accuracy over extended distances (Ali et al., 2022; Muhammad et al., 2020). Therefore, appropriate mitigation strategies must be implemented to ensure the simultaneous preservation of transmission quality and reliable sensor signal detection.

Numerous studies have extensively investigated the co-existence of FBG sensors and optical communication systems. Senkans et al., 2019 demonstrated the feasibility of a combined FBG sensing and 1.5 Gbit/s transmission system over 20 km of a single-strand single-mode fiber (SMF) using a shared light source, achieving a bit error rate (BER) of 6.1×10^{-7} through both simulation and experimental validation (Senkans et al., 2019). Braunfelds et al., 2021 investigated the integration of FBG sensors into optical communication networks without any additional dispersion compensation technique. The system's performance was analyzed using eye diagrams for NRZ-OOK modulation at 10 Gbit/s over transmission distances of 20 and 40 km, with and without the integrated FBG sensor. The results indicated that the presence of the FBG sensor did not degrade signal quality; however, dispersion effects became evident in the eye diagram after the 40 km transmission. Furthermore, the authors examined the integration of five FBG sensors within a 32-channel passive optical network (PON) system with 20 km of fiber length. System performance was evaluated through simulations, focusing on data transmission employing pre compensation via dispersion compensating fiber (DCF). The findings suggested that the inclusion of FBG sensors had a negligible impact on data channel signal quality, yielding a BER of 3.72×10^{-7} (Braunfelds et al., 2021).

Firdaus et al., 2022 evaluated two FBG sensors over 80 km of fiber link with a post DCF configuration and observed strong communication performance and well-defined reflections with a peak Q-factor of 4.87 and BER of 4.3×10^{-7} (Firdaus et al., 2022). Complementing these fiber-based systems, Hayle et al., 2022 experimentally demonstrated a 2.5 Gb/s free-space optical (FSO) link integrated with three intensity and wavelength division multiplexing (IWDM)-based FBG sensors, utilizing a broadband light source for both data and sensing. The system showed only $\tilde{1}$ dB power degradation at a BER threshold of 10^{-9} compared to the back-to-back configuration (Hayle et al., 2022). In a hybrid FSO-fiber setup, Dehnaw et al., 2023 incorporated four FBG sensors with coarse wavelength division multiplexing (CWDM) technology, analyzing system quality through error vector magnitude (EVM) and constellation diagrams across various scenarios. The system maintained an EVM of 4.03% at a maximum distance of 35 km SMF and 2 m of FSO, underscoring the robustness of FBG integration within multiplexed optical environments (Dehnaw et al., 2023).

Although previous studies have investigated dual-function fiber systems, only a few have demonstrated successful transmission over distances shorter than 120 km that embed multiple FBG sensors while still maintaining both high-speed telecommunication and distributed sensing integrity using a broadband source. This study investigates the dual-functionality of a 120 km SMF system that transmits 10 Gbps data while simultaneously supporting FBG-based sens-

ing. This length threshold is selected not arbitrarily but in alignment with spans for regional networks, where the impact of chromatic dispersion becomes more significant and dispersion compensation must be carefully optimized. Three FBG sensors with center wavelengths of 1554, 1556, and 1558 nm were positioned at 30 km intervals and interrogated using a broadband amplified spontaneous emission (ASE) source that simultaneously delivered the 1550 nm data signal. The adoption of a broadband ASE source eliminates the need for multiple discrete lasers or wavelength-division multiplexing (WDM) components, thereby streamlining the system architecture.

The system is evaluated using standard optical communication metrics, i.e., Q-factor, BER, and eye diagrams, alongside measurements of reflected power from each FBG. To maintain signal integrity, DCF is incorporated as its simplicity, stability, widespread use, cost-effectiveness, and proven reliability make it an ideal choice for scalable long-haul networks (Sakthivel et al., 2024; Neheeda et al., 2016). In addition, the system is assessed under three (pre-, post-, and symmetrical) DCF configurations, following the previous comparative framework (Ranathive et al., 2022). The results show that the presence of FBG sensors has minimal impact on data transmission. The post compensation setup achieved the most favorable performance across all operating conditions, ensuring robust signal integrity within the integrated system while preserving well-defined and clearly distinguishable sensor reflections throughout the system.

To the best of our knowledge, this is the first study to demonstrate multi-FBG sensors over a 120 km of single-strand optical fiber using a single broadband light source, effectively combining high-speed data communication and distributed sensing within a unified architecture. The results confirm a simulation-validated, co-functional optical system for long-distance operation with minimal hardware complexity, well suited to cost-sensitive, space-limited deployments in subsea and remote settings. This approach enables a single optical link for high-speed communication and distributed sensing, providing a scalable SMART infrastructure capable of bridging the digital divide and delivering life-saving tsunami early warnings to Indonesia's remote, sparsely populated, and seismically active islands.

2. Methods

A simulation study was conducted to investigate and assess the efficacy of the FBG sensors incorporated into a 120 km optical transmission system, employing OptiSystem v.18. Three FBG sensors are integrated into the transmission link, and the influence of various DCF configurations and system disturbances on the overall performance is systematically investigated.

2.1 System Design

The system architecture comprises three main subsystems: transmitter, optical fiber link with integrated sensors, and receiver segments. The FBG sensors are integrated at 30 km intervals along an SMF, resulting in a total transmission length of 120 km, as shown in Figure 1.

An ASE light source operating within the C-band (1546–1560 nm) centered at 1553 nm is employed to support both telecommunication and sensing functions. The ASE source is intentionally selected to evaluate the feasibility of resource-sharing in cost-constrained or infrastructure-limited environments. While laser-based sources offer higher coherence for data transmission, the spectrum-sliced wavelength division multiplexing (SS-WDM) technology offered by ASE source enables simultaneous support of multiple wavelengths (Senkans et al., 2019), aligning with the spectral needs of both the data channel and FBG interrogation wavelengths. This scenario is not intended to reflect commercial deployment practice but rather to test the fundamental performance limits of a unified light source architecture. The launch power is varied from 5 to 15 dBm in 2 dBm increments, a range extensively studied for its effectiveness in mitigating dispersion in optical communication systems (Odeh, 2023; Qureshi et al., 2020; HU et al., 2010). The optical output is directed to a 20:80 power splitter, enabling efficient

power allocation between the telecommunication and sensing channels (Purnamaningsih et al., 2016), in which 80% of the optical power is routed to a rectangular tunable optical band-pass filter (OBPF) centered at 1556 nm, with an 8 nm bandwidth spanning 1552–1560 nm, precisely matching the FBG sensors' interrogation range. This filtering enhances the spectral alignment, signal fidelity, and overall interrogation efficiency, thereby improving the sensing accuracy and system stability. The remaining 20% of the optical power is directed to an arrayed waveguide grating (AWG), which isolates the 1550 nm wavelength, which was previously identified as optimal for high-speed telecommunication data transmission (Rahmadiansyah et al., 2022).

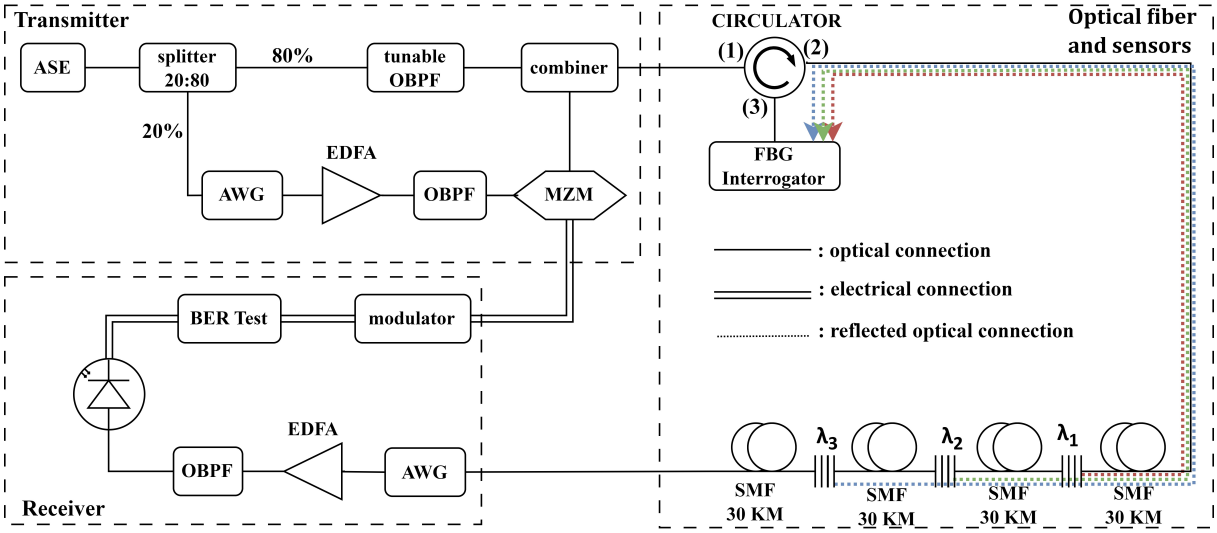

Figure 1 Basic Design of the proposed dual-function optical fiber system integrating high-speed communication and FBG-based sensing

To preserve signal quality, the isolated 1550 nm channel is amplified using a 20 dB erbium-doped fiber amplifier (EDFA) and further refined with a Gaussian OBPF to suppress unwanted spectral components. This dual-stage signal conditioning process ensures that only the intended telecommunication wavelength reaches the receiver, thereby enhancing signal quality, leading to a better signal-to-noise ratio (SNR) and reducing BER, consistent with the findings of Chen et al. (Chen et al., 2009). Overall, this integrated approach enables the efficient coexistence of high-precision optical sensing and high-speed telecommunication within a unified fiber-optic infrastructure, supporting stable and high-quality system performance.

The output signal from the Gaussian OBPF is subsequently modulated by a mach-zehnder modulator (MZM) driven by a 10 Gbit/s Non-Return-to-Zero (NRZ) data stream generated by a pseudo-random bit sequence (PRBS) generator. The NRZ format is selected as a baseline standard owing to its extensive utilization (Firdaus et al., 2022; Braunfelds et al., 2021; Senkans et al., 2019), compatibility with intensity-modulated direct detection (IM-DD) systems and relative ease of implementation in comparison to alternative modulation techniques. Unlike NRZ data transmission, which requires a narrowband optical carrier, an ASE source inherently exhibits a broad spectral range. To address this mismatch, the ASE output is spectrally filtered using an OBPF and an AWG prior to modulation by the MZM. This filtering process effectively isolated the data carrier and suppressed out-of-band noise, thereby enhancing the optical signal-to-noise ratio (OSNR) before modulation.

The modulated telecommunication signal is then combined with the sensing signals via a combiner. This composite signal enters port 1 of an optical circulator (OC), which separates forward- and backward-propagating light. Forward signals are transmitted through port 2 into a single optical fiber hosting multi-FBG sensors, each reflecting a distinct Bragg wavelength. The reflected wavelengths, encoded with sensing data, return to the OC and are routed to port 3, where they are analyzed with a WDM FBG interrogator to extract spectral shifts for

sensing diagnostics. The FBG_s are conceptualized as ideal reflective filters precisely centered with their corresponding Bragg wavelengths. The FBG wavelength shifts are detected through the observation of the reflected light along the optical fiber, where fluctuations in external factors such as strain or temperature influence the Bragg wavelength, leading to a quantifiable variation in the reflected signal. Furthermore, the system's ability to differentiate multiple FBG reflections across various spectral locations and to dynamically monitor the wavelength shifts simulated and analyzed to ascertain both the distinguishability and integrity of the spectral data.

On the communication side, the system performance is assessed using a BER tester. The received signal is first filtered by an AWG to isolate the 1550 nm telecommunication channel, then amplified by an EDFA and further refined by a Gaussian OBPF to suppress the ASE noise. The resulting cleaned optical signal is converted into an electrical signal via a photodetector (PD). A modulator provides a synchronized reference signal to the BER tester, enabling accurate evaluation of data transmission integrity.

Furthermore, a 1-km segment of the DCF with a high negative dispersion coefficient is employed to counterbalance the accumulated positive chromatic dispersion from the standard SMF. This compensation is critical for preserving signal integrity and mitigating pulse broadening over extended transmission distances. For effective dispersion management, these conditions must be satisfied:

Where D represents the dispersion parameter (ps/nm/km) and L denotes the length of the respective fiber segment (Meena and Kumar-Gupta, 2019). In this study, three DCF configurations, i.e., pre-, post-, and symmetrical compensation, are explored as part of a comparative analysis to identify the most effective placement strategy within the proposed system architecture (Sabri et al., 2024; Odeh, 2023; Jyotsana et al., 2014). Figure 2 shows a simplified representation of the simulated DCF placement schemes (a) pre-, (b) post-, and (c) symmetrical compensation.

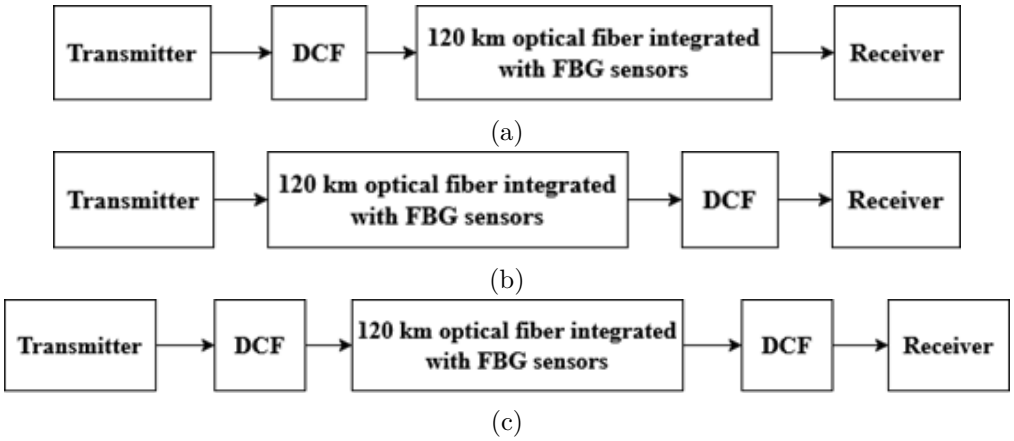

Figure 2 Architectures of a 120 km optical transmission system integrating FBG sensors with different DCF placement schemes: (a) pre-, (b) post-, and (c) symmetrical compensation schemes

In the pre compensation configuration, the DCF is placed before the optical fiber segment containing the FBG sensors, immediately following the EDFA in the transmitter section. This setup enables early correction of chromatic dispersion across all operational wavelengths, covering both telecommunication and sensor signals, prior to transmission through the main fiber span.

In contrast, the DCF is positioned after the sensor-integrated optical fiber and just before the receiver section in the post compensation configuration. Here, dispersion accumulated throughout the transmission path is fully corrected before signal demultiplexing and filtering, ensuring that the 1550 nm telecommunication channel arrives at the receiver with minimal distortion.

The symmetrical compensation scheme combines both approaches by placing two DCF

segments, one preceding and one following the FBG-integrated span. Each segment provides half of the total required dispersion compensation while maintaining the same net dispersion as in the pre- and post compensation schemes. This balanced architecture supports improved dispersion management and allows for a consistent performance comparison across all three DCF placement strategies within a long-haul optical communication system integrated with FBG sensor networks.

2.2 Predefined Parameters

Our simulation is conducted under predefined parameter conditions, including those for the FBG sensors, DCF modules, and system-wide configurations, to ensure consistency and reliability in evaluating the overall system performance.

Table 1 Specifications of the FBG sensors used in the simulation

Parameters	FBG $\lambda 1$	FBG $\lambda 2$	FBG $\lambda 3$
Center wavelength [nm]	1554	1556	1558
Reflectivity [%]	90	90	90
Bandwidth [nm]	0.1	0.1	0.1
Fiber type	SMF	SMF	SMF
Temperature reference [°C]	20	20	20
Temperature range [°C]	$-40-120$	$-40-120$	$-40-120$

Three FBG sensors, each with a reflectivity of 90% as detailed in Table 1, were selected to ensure effective reflection of their respective operational wavelengths, which is particularly critical for deployment within a long-haul optical communication system. The FBG specification employed in this system operates over a temperature range from -40°C to 120°C (Technica, 2018), and the temperature is varied at intervals of 60°C, with a reference temperature initially set at 20°C. This approach facilitates a systematic evaluation of the thermal responsiveness of the sensor through the application of extreme temperatures (which do not cause physical damage to the sensor) and ambient temperature, thus guaranteeing consistent evaluations across a defined operational spectrum.

Table 2 summarizes the optical fiber properties applied in the simulation. The SMF specifications conform to the ITU-T G.652 standard, while the DCF module parameters are derived analytically to meet the system's dispersion compensation requirements.

Table 2 SMF and DCF modules' Parameters

Cable Parameters	SMF	DCF
Dispersion [ps/nm/km]	16.75	-2010
Dispersion slope [ps/(nm^2/km)]	0.075	0.075
Attenuation [dB/km]	0.2	0.5

Table 3 outlines the system-wide parameters defined to ensure methodological consistency across all simulation stages. Three key metrics are analyzed to evaluate the performance of the telecommunication system operating at 1550 nm: Q-factor, BER, and eye diagram characteristics. In the preliminary evaluation, a 128-bit PRBS sequence is employed to strike an optimal balance between simulation complexity and statistical validity, providing sufficient bit-pattern diversity for initial BER assessment while minimizing computational overhead. This configuration is consistent with simulation methodologies reported in earlier studies (Odeh, 2023; Xia et al., 2019; Patnaik and Sahu, 2013). To improve the reliability and statistical robustness of the BER assessment, the sequence length is increased to 1,024 bits during the full evaluation

of the integrated system, yielding a more accurate representation of the error distribution. In parallel, FBG sensing performance is characterized by measuring reflected signal levels and assessing wavelength shifts induced by temperature variations. Combined, these evaluations offer a comprehensive view of signal integrity, system reliability, and data transmission quality across the three DCF configurations and multiple FBG integration scenarios.

Table 3 System-Wide Simulation Parameters

Parameters	Values
Reference wavelength [nm]	1550
Length of SMF [km]	120
Channel bit rate [Gbit/s]	10
Sequence length [bits]	128, 1024
Samples per bit	128, 32
Injected power [dBm]	$5-15$

3. Results and Discussion

In this work, we explored the interplay between universal optical communication and distributed optical sensing within a unified fiber infrastructure. A 120 km single-mode optical transmission link was modeled, incorporating three FBG sensors positioned at regular intervals to emulate an integrated communication-sensing system. Three DCF arrangements, i.e., pre-, post-, and symmetrical positions, were evaluated not as primary focus, but as contextual baselines to assess their effect on system stability and data integrity in the presence of sensing elements. To disentangle the contribution of the sensing architecture, we compared these results with an equivalent reference system without FBG_s. This dual-layered analysis aims to inform early-stage design strategies for future deployments of fiber-optic systems where high-speed data transmission must coexist with embedded environmental or structural monitoring capabilities.

The system's performance assessment is anchored on three interdependent metrics: Q-factor, BER, and eye diagram morphology. These parameters are intrinsically linked and collectively capture the fidelity of optical signal transmission. The Q-factor, a statistical measure of signal discrimination, is directly correlated with the eye diagram's opening extent, serving as a visual proxy for noise margin and jitter tolerance. A broader eye aperture signifies reduced intersymbol interference and enhanced temporal resolution, resulting in a higher Q-factor. Consequently, the BER exhibits an inverse relationship, with lower values indicating greater robustness against transmission impairments and improved signal integrity across the optical link (Hugar et al., 2024).

To support the preliminary analysis, Table 4 summarizes the BER performance results of the optical fiber system utilizing three dispersion compensation schemes, which were taken without the FBG_s. The evaluation spans injected optical power levels ranging from 5 to 15 dBm, offering a dynamic view of the system's resilience under varying launch conditions. Complementing the BER data, the table presents the associated Q-factor, eye height, and received power for each configuration, forming a multidimensional representation of transmission fidelity. Notably, the inclusion of received power metrics serves a critical role in delineating the receiver's dynamic range and identifying potential overload thresholds that could compromise signal integrity. This holistic approach enables a more nuanced understanding of how each compensation scheme interacts with both the physical layer and receiver-side performance limits.

Table 4 BER performance of a 120 km optical transmission system (taken without FBG$_s$) under different DCF compensation configurations.

DCF Configurations	Injected Power [dBm]	Q-factor	BER	Eye Height	Received Power [dBm]
Pre	5	11.10	4.30×10^{-29}	4.67×10^{-4}	-5.11
	7	15.17	2.06×10^{-52}	1.01×10^{-3}	-2.25
	9	16.72	3.26×10^{-63}	1.60×10^{-3}	-0.35
	11	19.61	4.53×10^{-86}	3.16×10^{-3}	2.44
	13	19.54	1.69×10^{-85}	2.98×10^{-3}	1.51
	15	10.64	8.30×10^{-27}	6.26×10^{-3}	6.18
Post	5	16.02	3.41×10^{-58}	1.20×10^{-3}	-1.55
	7	11.33	2.95×10^{-30}	4.97×10^{-4}	-4.96
	9	20.44	2.74×10^{-93}	2.60×10^{-3}	1.61
	11	24.66	1.05×10^{-134}	3.90×10^{-3}	3.22
	13	20.91	1.49×10^{-97}	3.97×10^{-3}	3.50
	15	19.27	3.45×10^{-83}	3.32×10^{-3}	2.49
Symmetrical	5	6.12	3.01×10^{-10}	1.41×10^{-4}	-9.56
	7	15.93	1.39×10^{-57}	1.11×10^{-3}	-1.82
	9	20.04	8.78×10^{-90}	1.23×10^{-3}	-1.59
	11	23.36	3.70×10^{-121}	3.33×10^{-3}	2.63
	13	14.17	5.17×10^{-46}	1.69×10^{-3}	0.15
	15	16.70	4.65×10^{-63}	2.17×10^{-3}	1.01

Figure 3 provides a graphical interpretation of key performance trends to enhance the quantitative results. Subfigure (a) shows the evolution of the Q-factor as a function of the injected optical power for each dispersion compensation scheme, offering insight into the interplay between the power level and signal fidelity. Subfigure (b) concurrently illustrates the corresponding received power, highlighting the receiver's susceptibility to saturation at higher launch powers. Together, these visualizations elucidate the operational envelope, i.e., balancing dispersion mitigation, signal integrity, and the onset of receiver overload, within which system performance remains optimal. Such insights are particularly valuable for the design of long-haul optical links where integrated FBG sensors impose additional constraints on power budgeting and spectral allocation.

As shown in Figure 3(a) and corroborated by the quantitative results in Table 4, the Q-factor exhibits a progressive enhancement with increasing injected optical power, reaching a performance apex near 11 dBm across all dispersion compensation configurations. This trend reflects improved SNR and temporal eye clarity under moderate launch conditions. However, beyond this optimal threshold, a notable decline in Q-factor is observed—marking the onset of nonlinear optical impairments, such as self-phase modulation and four-wave mixing, which become increasingly pronounced in long-haul transmission (Amiri et al., 2023; Syuaib et al., 2018; Asvial and Paramitha, 2015). These findings underscore the critical need to define a carefully balanced launch power that maximizes transmission fidelity while safeguarding system stability against nonlinear degradation.

Upon closer examination of Figure 3(a) and 3(b), subtle inconsistencies emerge in the observed performance trends, showing minor irregularities in the system's optical behavior. These deviations are plausibly attributed to the spectral characteristics of the superluminescent light emitting diode (SLED) employed as the broadband ASE source. While SLEDs are well-suited for sensing applications due to their wide spectral bandwidth and low coherence noise,

their inherently non-coherent nature makes them less ideal for long-haul optical communication systems, where narrow spectral linewidths and high coherence—typically offered by laser-based sources—are essential for maintaining transmission fidelity (Zhang et al., 2019; Rossetti et al., 2012).

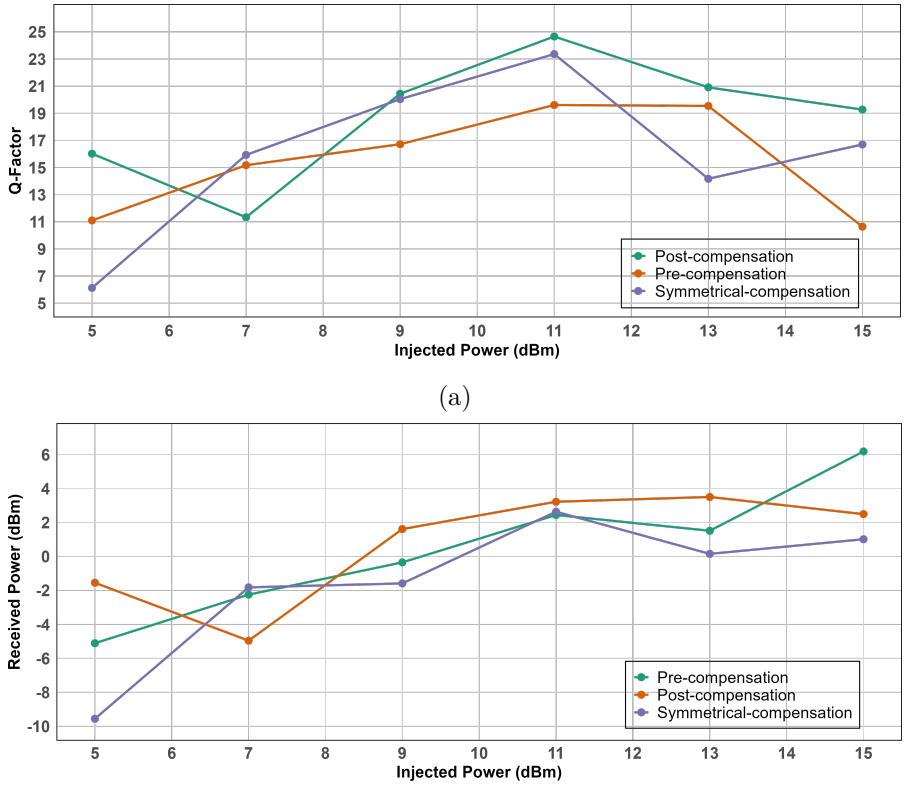

Figure 3 Comparison of the influence of injected optical power on system performance: (a) injected power vs. Q-factor and (b) injected power vs. received power

Despite these limitations, the proposed system demonstrates consistent performance behavior across all dispersion compensation configurations evaluated. Notably, each scheme exhibited optimal performance at an injected optical power of approximately 11 dBm. At this power level, the respective Q-factors are recorded at 19.61 for pre compensation, 24.66 for post compensation, and 23.36 for symmetrical compensation. Among these, the post compensation configuration delivers the most favorable results, achieving the highest Q-factor, the lowest BER (1.05×10^{-134}), and a distinctly open-eye diagram (Figure 4). Nevertheless, it is important to note that the exceptionally low BER values obtained in this preliminary evaluation are partly attributable to the relatively short sequence length employed. For the initial analysis of BER and eye diagrams under error-free conditions, a 2^7-1 PRBS sequence was deemed theoretically sufficient, as it offers adequate variability in bit patterns while minimizing computational overhead and reducing simulation time. To enable a more accurate and statistically robust BER assessment, the integrated system evaluation subsequently employed a longer PRBS sequence of 1,024 bits, providing a larger sample size and a broader range of bit patterns. This approach ensures a more representative and reliable characterization of the overall system performance.

Considering the optimal performance observed at an optical launch power of 11 dBm in the baseline system, this value is subsequently adopted as the reference input power for simulations involving the optical fiber system integrated with FBG-based sensing. This ensures consistency in performance evaluation and facilitates direct comparison across configurations.

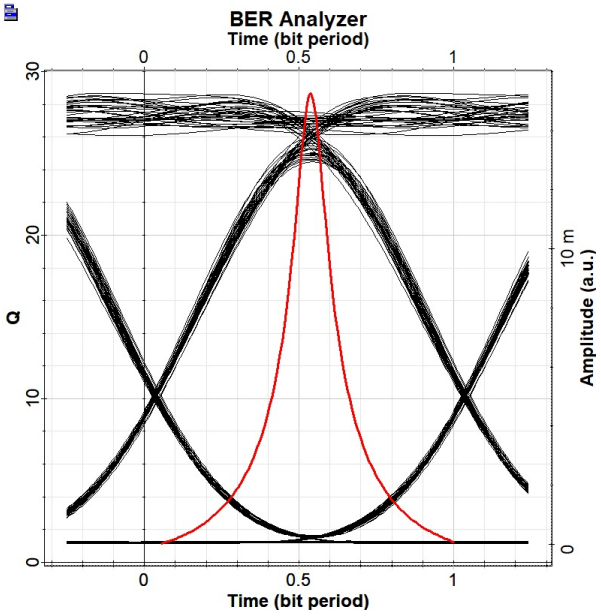

Figure 4 Eye pattern obtained from the BER analyzer under post compensation configuration with 11 dBm injected optical power

Table 5 BER simulation results on optical fiber integrated with FBG sensors; compensated

DCF Configurations	Bit Sequence [Bits]	Q-factor	BER	Eye Height	Received Power [dBm]
Pre	128	14.90	1.33×10^{-50}	1.99×10^{-3}	1.58
	1024	5.93	1.08×10^{-09}	1.57×10^{-4}	-8.01
Post	128	19.29	2.98×10^{-83}	7.44×10^{-3}	3.29
	1024	6.38	6.23×10^{-11}	2.11×10^{-4}	-6.58
Symmetrical	128	18.98	1.09×10^{-80}	3.87×10^{-4}	3.30
	1024	4.61	1.43×10^{-06}	6.19×10^{-5}	-10.44

Table 5 presents the BER performance of the distributed optical fiber architecture integrated with the FBG-based sensing system under two different bits sequence length. The results indicate that increasing the bit sequence length reduces the BER, thereby improving the statistical robustness of the measurement and providing a more accurate representation of the system's intrinsic error performance. Across all DCF configurations, the BER of the telecommunication channel remains well below the pre–forward error correction (FEC) threshold specified in ITU-T G.975.1 ($\leq 2 \times 10^{-3}$) (International Telecommunication Union, 2004). Consistent with the results observed in systems without integrated sensors, the post compensation configuration demonstrates the best overall performance, achieving a Q-factor of 6.38 and a corresponding BER of 6.23×10^{-11} at a bit-sequence length of 1,024. Meanwhile, the received optical power measured at -6.58 dBm, may serve as a practical reference for the receiver's overload threshold in future experimental configurations targeting BER optimization.

Figure 5 compares the eye diagram quality of the telecommunication signal under different sequence lengths. When analyzed along the vertical and horizontal axes, the eye diagram reflects amplitude margins and timing intervals, respectively. Figure 5(a) shows that the pattern obtained using a 128-bit sequence remains distinctly open and symmetric, indicating low noise levels and minimal intersymbol interference. However, the diagram exhibits noticeable degradation as the sequence length increases, likely due to noise and timing jitter introduced by the larger statistical sample and the broader spectrum of bit patterns. This results in a more closed eye pattern, as illustrated in Figure 5(b).

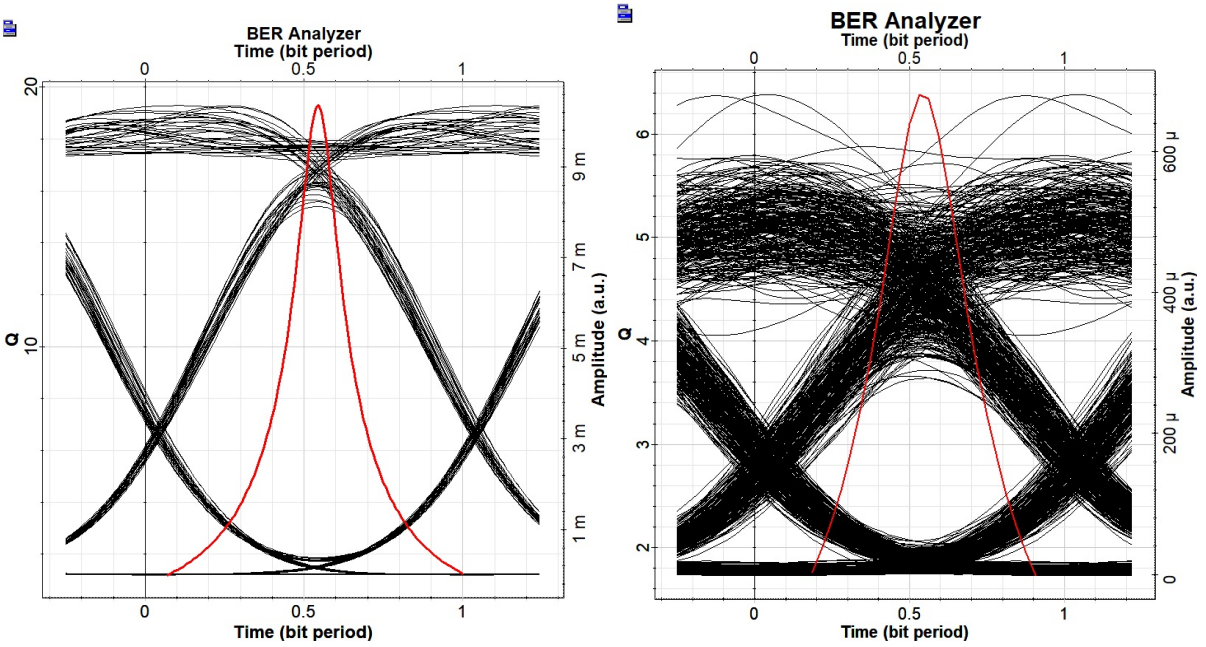

(a) (b)

Figure 5 Eye diagram obtained from the BER analyzer for the optical fiber system incorporating FBG sensors: (a) 128 bits sequence; (b) 1024 bits sequence

Both findings eventually confirmed that the presence of FBG sensors introduces no discernible impairment on signal integrity, underscoring the viability of seamlessly integrating high-speed telecommunications and distributed sensing within a shared optical fiber infrastructure without compromising performance. A detailed follow-up analysis is performed to evaluate the reflected sensor signals influenced by each DCF configuration, as well as the effect of temperature variations, on the FBG wavelength shifts, as captured by the WDM FBG interrogator. Three distinct reflection peaks are clearly observed at 1554, 1556, and 1558 nm, each exhibiting varying power levels contingent on the specific DCF scheme, as shown in Figure 6.

Furthermore, a residual spectral component centered at 1550 nm, corresponding to the telecommunication carrier (denoted as marker D), is identified in Figure 6. This signal appears with a markedly low intensity of approximately -72.78 dBm, suggesting negligible back-reflection and minimal crosstalk with the sensor wavelengths. Collectively, these findings reinforce the operational compatibility of high-speed telecommunication and distributed sensing when co-located within a single optical fiber strand, supporting the practicality of hybrid system deployment.

These results affirm that the incorporation of FBG sensing does not compromise the integrity of the telecommunication channel, nor does the presence of high-speed data transmission impede the fidelity or detectability of the FBG reflections. This demonstrated mutual transparency between sensing and communication functions underscores the feasibility of simultaneous operation within a unified optical fiber infrastructure, paving the way for integrated systems that support both data transport and distributed sensing without performance degradation.

As presented in Table 6, the first FBG sensor, centered at a wavelength of 1554 nm and positioned closest to the interrogator, exhibited the highest reflected signal intensity relative to the subsequent sensors. The spatial distribution of the FBG$_s$ at uniform 30 km intervals revealed a consistent attenuation pattern, with signal levels decreasing by approximately 12 dB between adjacent sensors. This trend is attributed to the intrinsic reflective nature of FBG sensors, in which each reflected signal must traverse twice the distance between the sensor and the interrogator. As a result, sensors positioned farther along the fiber experience greater optical loss, leading to progressively diminished signal strength. This distance-dependent attenuation is particularly evident in the last sensor, whose signal undergoes the longest round-trip propagation, thus exhibiting the lowest power level among the group.

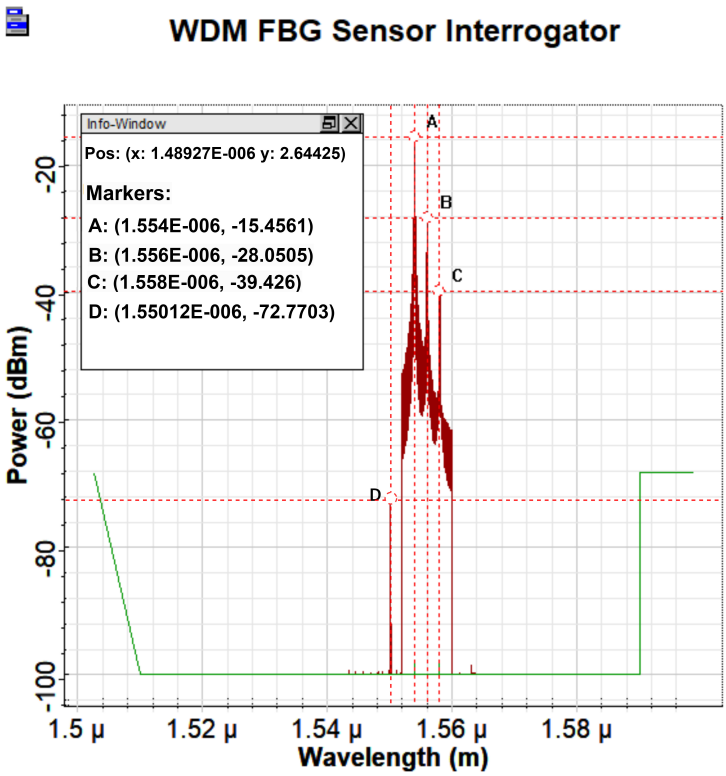

Figure 6 Reflected wavelength outputs from the FBG sensor interrogator under the post-compensation scheme

Table 6 FBG reflected signals simulation result; compensated

DCF Configurations	1st signal [dBm]	2nd signal [dBm]	3rd signal [dBm]
Pre	-15.81	-27.94	-39.46
Post	-15.46	-28.05	-39.43
Symmetrical	-15.21	-28.10	-39.22

A comparative evaluation of the FBG sensor performance across different DCF configurations is depicted in Figure 7. The results indicate that the choice of DCF scheme exerts no significant impact on the quality of the reflected FBG signals, as evidenced by the relatively uniform signal levels across all configurations. This proves that the reflective performance of the FBG sensors remains stable regardless of the dispersion management approach employed. The minor variations observed among the three cases further highlight the robustness of the sensor system under diverse dispersion conditions.

Further evaluation of the sensing performance is conducted, particularly to assess the influence of temperature fluctuations implemented in this system, providing a more comprehensive analysis of the FBG$_s$' performance. As illustrated in Figure 8, the Bragg wavelengths display systematic shifts that align with temperature variations of -40°C, 20°C, and 80°C. These changes yield Bragg wavelength deviations of approximately 0.8–0.9 nm relative to their wavelengths at a reference temperature of 20°C. Such changes alter the grating period of the FBG and induce thermal expansion of the optical fiber, collectively modifying the fiber core's effective refractive index.

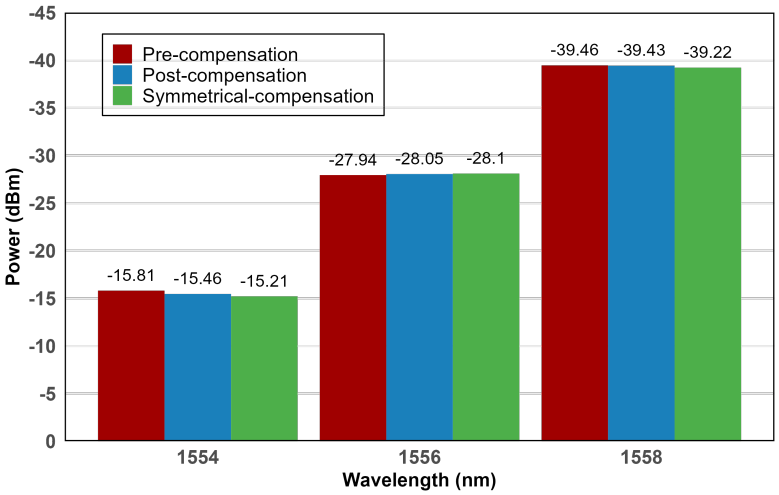

Figure 7 Comparison of reflected signals from FBG sensors under different DCF compensation configurations

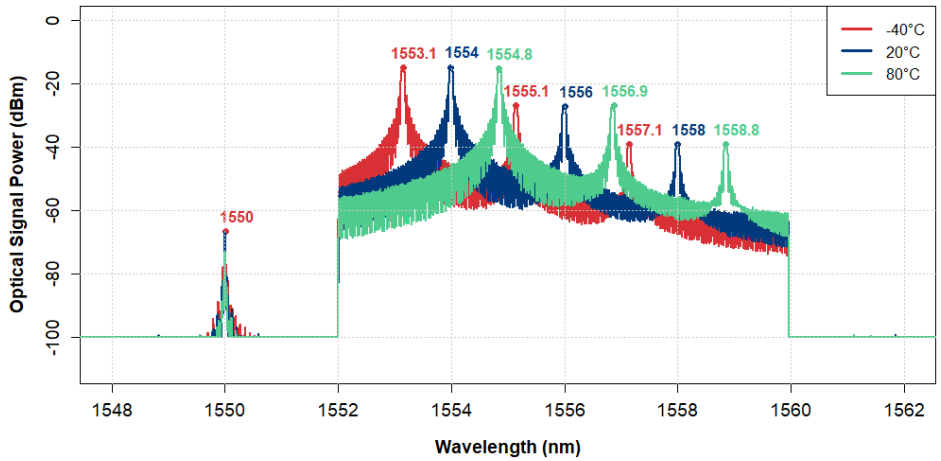

Figure 8 Wavelength shifts of FBG in relation to temperature variations

Figure 8 also demonstrates that the telecommunication signal experiences negligible degradation and produces no measurable crosstalk, whereas the sensor signals maintain effective responsiveness to the temperature variations within the system. Beyond confirming compatibility, this co-integration paradigm delivers tangible economic benefits, with the potential to significantly reduce capital and operational expenditure through infrastructure consolidation, optimized resource utilization, and dual functionality. In this study, a 120 km SMF link operating at 10 Gbps with NRZ-OOK modulation and a broadband ASE light source was successfully combined with three FBG-based sensors, achieving uncompromised performance in both data transmission and distributed sensing. These outcomes not only validate the technical feasibility of a unified fiber network but also set a new performance benchmark for converged communication–sensing architectures, offering a scalable and robust framework for next-generation SMART systems. As summarized in Table 7, the proposed system surpasses the capabilities reported in prior work, highlighting its potential as a pivotal enabler for future intelligent network infrastructures.

Table 7 Results comparison of dual-function systems

Study	Transmission Distance	Bit rate [Gbit/s]	Modulated Signal	Light Source	No. of FBG	BER
Senkans et al., 2019	20 km SMF	1.5	NRZ-OOK	Broadband ASE	1	6.1×10^{-7}
Braunfelds et al., 2021	20, 40 km SMF	10	NRZ-OOK	Broadband ASE	1	NA
Firdaus et al., 2022	20 km SMF	10	NRZ-OOK	Broadband ASE	5	3.72×10^{-7}
	80 km SMF	10	NRZ-OOK	Broadband ASE	2	4.3×10^{-7}
Hayle et al., 2022	2 m Free atmospheric turbulence environment	2.5	NA	Broadband LS (BLS)	3	10^{-5}
Dehnaw et al., 2023	35 km SMF and 2 m of FSO	NA	NA	Separated Source	4	NA
This work (2025)	120 km SMF	10	NRZ-OOK	Broadband ASE	3	6.23×10^{-11}

4. Conclusions

This study evaluated a 120 km optical fiber system integrating high-speed telecommunication and embedded FBG sensors, an architecture envisioned to support next-generation SMART infrastructure. With three FBGs spaced at 30 km intervals, the system enabled simultaneous data transmission and distributed sensing over a single optical path. Simulation results confirmed the feasibility of this dual-function design, achieving optimal performance at a launch power of 11 dBm, with a Q-factor of 6.38, and a BER of 6.23×10^{-11}. Among the tested dispersion compensation strategies, post compensation yielded the most favorable data transmission performance, whereas FBG signal integrity remained robust across all configurations. The results further reveal that the telecommunication signal experiences negligible degradation and no measurable crosstalk, while the sensor signals maintain effective responsiveness to temperature variations. These findings underscore the technical viability and reliability of sensing and communication co-location within a single fiber link. Although the simulation results are promising, the study is limited by idealized assumptions that exclude real-world factors such as component imperfections, nonlinear optical effects, and environmental disturbances. The linear, uniformly spaced sensor layout does not reflect the spatial complexity of real deployments. Moreover, the assumed coexistence of sensing and communication requires empirical validation under operational conditions. Future work should prioritize experimental prototyping and field trials with a focus on denser sensor arrangements, adaptive dispersion control, and power efficiency. These efforts are essential for realizing cost-effective, multifunctional optical networks that integrate high-speed communication with distributed sensing.

Acknowledgements

This research is supported by Program Riset dan Inovasi untuk Indonesia Maju (RIIM) LPDP Grant and BRIN, grant number (G3) No: RIIM-30141557602.

Author Contributions

Conceptualization: Sasono Rahardjo. **Methodology**: Mustika Fitriana Dewi, Muhammad Yusha Firdaus. **Validation**: Muhammad Yusha Firdaus, Mustika Fitriana Dewi. **Formal analysis**: Mustika Fitriana Dewi, Muhammad Yusha Firdaus, Muhamad Asvial, Agus Muhamad Hatta. **Investigation**: Maratul Hamidah, Tinova Pramudya. **Data Curation**: Rahmayati Alindra, Amalia Irma Nurwidya. **Writing - Original Draft**: Mustika Fitriana Dewi. **Writing - Review & Editing**: Maratul Hamidah, Rahmayati Alindra. **Visualization**: Tinova Pramudya, Amalia Irma Nurwidya. **Supervision**: Sasono Rahardjo, Muhamad Asvial, Agus Muhamad Hatta. **Funding acquisition**: Sasono Rahardjo.

Conflict of Interest

The authors declare no conflicts of interest.

References

Ali, R. S., Fattah, A. Y., & Hassib, M. D. (2022). The effects of optical fiber impairments on communication systems. *Indonesian Journal of Electrical Engineering and Computer Science*, *28*(1), 241–253. https://doi.org/10.11591/ijeecs.v28.i1.pp241-253

Amiri, I., Rashed, A. N. Z., Mohamed, A. E. A., Aboelazm, M. B., & Yupapin, P. (2023). Nonlinear Effects with Semiconductor Optical Amplifiers. *Journal of Optical Communications*, *44*(1), 11–17. https://doi.org/10.1515/joc-2019-0053

Asvial, M., & Paramitha, M. P. (2015). Analysis of high order dispersion and non linear effects in fiber optic transmission with Non Linear Schrodinger Equation model. *2015 International Conference on Quality in Research (QiR)*, 145–150. https://doi.org/10.1109/QiR.2015.7374915

Braunfelds, J., Spolitis, S., Porins, J., & Bobrovs, V. (2021). Fiber Bragg Grating Sensors Integration in Fiber Optical Systems. In *Application of optical fiber in engineering*. IntechOpen. https://doi.org/10.5772/intechopen.94289

Chen, Y., Mark, B. L., Burnham, R., & Verdun, H. (2009). Reducing ASE Effect in Coherent Detection by Employing Double-Pass Fiber Preamplifier and Time-Domain Filter. *IEEE Journal of Quantum Electronics*, *45*(10), 1289–1296. https://doi.org/10.1109/JQE.2009.2024773

de la Torre, O., Floris, I., Sales, S., & Escaler, X. (2021). Fiber Bragg Grating Sensors for Underwater Vibration Measurement: Potential Hydropower Applications. *Sensors*, *21*(13), 4272. https://doi.org/10.3390/s21134272

Dehnaw, A. M., Manie, Y. C., Du, L.-Y., Yao, C.-K., Jiang, J.-W., Liu, B.-X., & Peng, P.-C. (2023). Integrated Sensor-Optics Communication System Using Bidirectional Fiber and FSO Channels and Hybrid Deep Learning Techniques. *Sensors*, *23*(20), 8434. https://doi.org/10.3390/s23208434

Elsherif, M., Salih, A. E., Muñoz, M. G., Alam, F., AlQattan, B., Antonysamy, D. S., Zaki, M. F., Yetisen, A. K., Park, S., Wilkinson, T. D., & Butt, H. (2022). Optical Fiber Sensors: Working Principle, Applications, and Limitations. *Advanced Photonics Research*, *3*(11). https://doi.org/10.1002/adpr.202100371

Firdaus, M. Y., Wibowo, D. K., Hamidah, M., Utama, R. P., Dewi, M. F., Hamdani, M., Setianingrum, L., Rahardjo, S., Purwoadi, M. A., & Purnomo, E. (2022). The Effect of Fiber Bragg Grating (FBG) Sensors on Data Channel of Fiber Optic Communication (FOC) System. *Proceedings of the 2022 International Conference on Computer, Control, Informatics and Its Applications*, 40–43. https://doi.org/10.1145/3575882.3575890

Hayle, S. T., Manie, Y. C., Yao, C.-K., Yeh, T.-Y., Yu, C.-H., & Peng, P.-C. (2022). Hybrid of Free Space Optics Communication and Sensor System Using IWDM Technique. *Journal of Lightwave Technology*, *40*(17), 5862–5869. https://doi.org/10.1109/JLT.2022.3186895

Howe, B. M., Angove, M., Aucan, J., Barnes, C. R., Barros, J. S., Bayliff, N., Becker, N. C., Carrilho, F., Fouch, M. J., Fry, B., Jamelot, A., Janiszewski, H., Kong, L. S. L., Lentz, S., Luther, D. S., Marinaro, G., Matias, L. M., Rowe, C. A., Sakya, A. E., ... Wilcock, W. (2022). SMART Subsea Cables for Observing the Earth and Ocean, Mitigating Environmental Hazards, and Supporting the Blue Economy. *Frontiers in Earth Science*, *9*. https://doi.org/10.3389/feart.2021.775544

Howe, B. M., Arbic, B. K., Aucan, J., Barnes, C. R., Bayliff, N., Becker, N., Butler, R., Doyle, L., Elipot, S., Johnson, G. C., Landerer, F., Lentz, S., Luther, D. S., Müller, M., Mariano, J., Panayotou, K., Rowe, C., Ota, H., Song, Y. T., ... Weinstein, S. (2019). SMART Cables for Observing the Global Ocean: Science and Implementation. *Frontiers in Marine Science*, *6*. https://doi.org/10.3389/fmars.2019.00424

HU, B., Jing, W., Wei, W., & Zhao, R.-m. (2010). Analysis on dispersion compensation with DCF based on Optisystem. *2010 2nd International Conference on Industrial and Information Systems*, 40–43. https://doi.org/10.1109/INDUSIS.2010.5565685

Hugar, N. R., P, P., Maleeha, & V, D. (2024). Simulation And Analysis of Bit Error Rate in Optical Fiber Communication Using Optisystem. *2024 7th International Conference on Devices, Circuits and Systems (ICDCS)*, 67–71. https://doi.org/10.1109/ICDCS59278.2024.10560832

International Telecommunication Union. *Forward error correction for high bit-rate DWDM submarine systems*. Recommendation G.975.1. 2004.

Jyotsana, Kaur, R., & Singh, R. (2014). Performance comparison of pre-, post- and symmetrical-dispersion compensation techniques using DCF on 40 Gbps OTDM system for different fibre standards. *Optik*, *125*(9), 2134–2136. https://doi.org/10.1016/j.ijleo.2013.10.059

Madani, N. A., Purnamaningsih, R. W., Poespawati, N. R., Hamidah, M., Rahardjo, S., & Wibowo, D. K. (2023). Detection of Low Hydrostatic Pressure Using Fiber Bragg Grating Sensor. *International Journal of Technology*, *14*(7), 1527. https://doi.org/10.14716/ijtech.v14i7.6714

Marra, G., Fairweather, D. M., Kamalov, V., Gaynor, P., Cantono, M., Mulholland, S., Baptie, B., Castellanos, J. C., Vagenas, G., Gaudron, J.-O., Kronjäger, J., Hill, I. R., Schioppo, M., Barbeito Edreira, I., Burrows, K. A., Clivati, C., Calonico, D., & Curtis, A. (2022). Optical interferometry–based array of seafloor environmental sensors using a transoceanic submarine cable. *Science*, *376*(6595), 874–879. https://doi.org/10.1126/science.abo1939

Meena, M. L., & Kumar-Gupta, R. (2019). Design and comparative performance evaluation of chirped FBG dispersion compensation with DCF technique for DWDM optical transmission systems. *Optik*, *188*, 212–224. https://doi.org/10.1016/j.ijleo.2019.05.056

Min, R., Liu, Z., Pereira, L., Yang, C., Sui, Q., & Marques, C. (2021). Optical fiber sensing for marine environment and marine structural health monitoring: A review. *Optics & Laser Technology*, *140*, 107082. https://doi.org/10.1016/j.optlastec.2021.107082

Muhammad, F., Ali, F., Habib, U., Usman, M., Khan, I., & Kim, S. (2020). Time Domain Equalization and Digital Back-Propagation Method-Based Receiver for Fiber Optic Communication Systems. *International Journal of Optics*, *2020*, 1–13. https://doi.org/10.1155/2020/3146374

Neheeda, P., Pradeep, M., & Shaija, P. J. (2016). Analysis of WDM System With Dispersion Compensation Schemes. *Procedia Computer Science*, *93*, 647–654. https://doi.org/10.1016/j.procs.2016.07.254

Nor, M. S. M., Khan, A. A., Mohamad, S., & Thirunavakkarasu, P. (2023). Development of Optical Fiber Sensor for Water Salinity Detection. *International Journal of Technology*, *14*(6), 1247. https://doi.org/10.14716/ijtech.v14i6.6650

Odeh, A. (2023). COMPARING DISPERSION COMPENSATION METHODS FOR 120 GB/S OPTICAL TRANSMISSION: PRE, POST, AND SYMMETRICAL SCHEMES. *The Journal of Engineering Research [TJER]*, *19*(2), 163–179. https://doi.org/10.53540/tjer.vol19iss2pp163-179

Patnaik, B., & Sahu, P. K. (2013). Optimized ultra-high bit rate hybrid optical communication system design and simulation. *Optik*, *124*(2), 170–176. https://doi.org/10.1016/j.ijleo.2011.11.080

Pendão, C., & Silva, I. (2022). Optical Fiber Sensors and Sensing Networks: Overview of the Main Principles and Applications. *Sensors*, *22*(19), 7554. https://doi.org/10.3390/s22197554

Priambodo, P. S., Rahardjo, S., Witjaksono, G., & Hartanto, D. (2015). Optimizing Coupling Region as Sensing Area in Optical Ring Resonator Sensor Applications. *International Journal of Technology*, *6*(4), 622. https://doi.org/10.14716/ijtech.v6i4.1271

Purnamaningsih, R. W., Raden Poespawati, N., Dogeche, E., & Pavlidis, D. (2016). A Simple Three Branch Optical Power Splitter Design based on III-Nitride Semiconductor for

Optical Telecommunication. *International Journal of Technology*, *7*(4), 701. https://doi.org/10.14716/ijtech.v7i4.3172

Qureshi, S., Qamar, F., Qamar, N., Shahzadi, R., Ali, M., Nadeem Khan, M. F., & Haroon, F. (2020). Bi-directional Transmission of 800 Gbps Using 40 Channels DWDM System for Long Haul Communication. *2020 3rd International Conference on Computing, Mathematics and Engineering Technologies (iCoMET)*, 1–7. https://doi.org/10.1109/iCoMET48670.2020.9073834

Rahmadiansyah, M., Anggraeni, S. P., Firdaus, M. Y., Dewi, M. F., Rahardjo, S., Rasuanta, M. P., Hamidah, M., Setianingrum, L., & Hatta, A. (2022). The Consideration of Attenuation and Chromatic Dispersion Parameters to Long-Haul Optical Communication. *Proceedings of the 2022 International Conference on Computer, Control, Informatics and Its Applications*, 50–54. https://doi.org/10.1145/3575882.3575892

Ranathive, S., Vinoth Kumar, K., Rashed, A. N. Z., Tabbour, M. S. F., & Sundararajan, T. V. P. (2022). Performance Signature of Optical Fiber Communications Dispersion Compensation Techniques for the Control of Dispersion Management. *Journal of Optical Communications*, *43*(4), 611–623. https://doi.org/10.1515/joc-2019-0021

Rossetti, M., Napierala, J., Matuschek, N., Achatz, U., Duelk, M., Vélez, C., Castiglia, A., Grandjean, N., Dorsaz, J., & Feltin, E. (2012). Superluminescent light emitting diodes: the best out of two worlds. *H. Schenk, W. Piyawattanametha, and W. Noell (eds)*, 825208. https://doi.org/10.1117/12.912759

Sabri, A. A., Jihad, N. J., & Hadi, W. A. H. (2024). Performance analysis of different dispersion compensation techniques in optical fiber communications system [Preprint]. *Journal of Optics*. https://doi.org/10.1007/s12596-024-01682-8

Sahota, J. K., Gupta, N., & Dhawan, D. (2020). Fiber Bragg grating sensors for monitoring of physical parameters: a comprehensive review. *Optical Engineering*, *59*(06), 1. https://doi.org/10.1117/1.OE.59.6.060901

Sakthivel, S., Mansoor Alam, M., Abu Bakar Sajak, A., Mohd Su'ud, M., & Riyaz Belgaum, M. (2024). Review of Compensation and Dispersion Techniques for Fiber Optic Lightpath Networks. *International Journal of Computing and Digital Systems*, *15*(1), 753–767. https://doi.org/10.12785/ijcds/160155

Senkans, U., Braunfelds, J., Lyashuk, I., Porins, J., Spolitis, S., & Bobrovs, V. (2019). Research on FBG-Based Sensor Networks and Their Coexistence with Fiber Optical Transmission Systems. *Journal of Sensors*, *2019*, 1–13. https://doi.org/10.1155/2019/6459387

Sifón, M. (2024). Science Monitoring And Reliable Technology (SMART) to monitor the ocean using submarine cables. *The International Hydrographic Review*, *30*(1), 172–177. https://doi.org/10.58440/ihr-30-1-n01

Suastika, K., Sahlan, S., Nugroho, W. H., Zubaydi, A., Misbah, M. N., & Murdjito, M. (2019). Fatigue Life Assessment of Waste Steel Reused as Tsunami Buoy Keel Structures: A Case Study. *International Journal of Technology*, *10*(4), 700. https://doi.org/10.14716/ijtech.v10i4.501

Syuaib, I., Asvial, M., & Rahardjo, E. T. (2018). Modeling of Ultra-Long Span Bidirectional Raman Transmission Link Using Three-Segment Hybrid Fiber Core Structure. *Photonics*, *6*(1), 2. https://doi.org/10.3390/photonics6010002

Technica. (2018). T830 In Line Temperature Sensor [Viewed 29 July 2025]. *Technica*. https://technicasa.com/t830-in-line-temperature-sensor/

Wang, B., Bai, Y., Chen, Q., Gao, H., Zhang, D., Jiang, L., & Qiao, X. (2023). Design and fabrication of a differential-pressure optical fiber grating sensor for monitoring the flow rate of fluid. *Applied Optics*, *62*(2), 385. https://doi.org/10.1364/AO.478649

Xia, P., Zhang, L.-H., & Lin, Y. (2019). Simulation Study of Dispersion Compensation in Optical Communication Systems Based on Optisystem. *Journal of Physics: Conference Series*, *1187*(4), 042011. https://doi.org/10.1088/1742-6596/1187/4/042011

Yu, J., Xu, P., Yu, Z., Wen, K., Yang, J., Wang, Y., & Qin, Y. (2023). Principles and Applications of Seismic Monitoring Based on Submarine Optical Cable. *Sensors*, *23*(12), 5600. https://doi.org/10.3390/s23125600

Zhang, T., Wang, W., Chen, H., Zhang, X., Ma, Z., & Lv, W. (2019). Extrinsic Fabry–Perot interferometric cavity-based fiber-optic spectrum equalization filter for the Gaussian spectrum of superluminescent diodes. *Applied Optics*, *58*(23), 6228. https://doi.org/10.1364/AO.58.006228